Neuro-deep fuzzy system for estimation of NO_2 concentration in soil and groundwater on highways from remote sensing images

Raja Shamayel Ullah[1], Junaid Ali Khan[1,2], Inzamam Mashood Nasir[3], Eunchan Kim[4,5], Hadeel Alsolai[6], Randa Allafi[7], Munya A. Arasi[8] and Faisal Mohammed Nafie[9]

[1] Department of Computer Science, HITEC University Taxila, Unaffiliated, Taxila, Pakistan
[2] Data Science and Analytics Department, Sakarya University, Sakarya, Turkey
[3] Faculty of Informatics, Kaunas University of Technology, Kaunas, Lithuania
[4] Department of Information Systems, Hanyang University, Seoul, Republic of South Korea
[5] Department of Artificial Intelligence, Hanyang University, Seoul, Republic of South Korea
[6] Department of Information Systems, College of Computer and Information Sciences, Princess Nourah Bint Abdulrahman University, Riyadh, Saudi Arabia
[7] Center for Scientific Research and Entrepreneurship, Northern Border University, Arar, Saudi Arabia
[8] Department of Computer Science, Applied College at RijalAlmaa, King Khalid University, Abha, Saudi Arabia
[9] Department of Natural and Applied Sciences, Community College, Majmaah University, Al Majmaah, Saudi Arabia

ABSTRACT

Remotely sensed data of the contaminated soil and groundwater near the highways around the mountains, deserts, sea side and agricultural fields are collected and analyzed by various traditional and modern techniques to take several purposeful decisions. This article presents a neuro-deep fuzzy system to estimate the concentration of nitrogen dioxide (NO_2) in the soil and nitric acid in the groundwater near the highways due to exhausts of gases from the motor vehicles. The proposed scheme is developed based on algebraic sum of Mexican hat wavelet function that is a universal approximator in the hidden layer's hybrid with a layer of fuzzy rules. The energy function is generated in an unsupervised manner based upon the diffusion of nitrogen dioxide in the soil surface and nitric acid in the water. A scenario-based case study on various highways has been developed by using various parametric values like air temperature, humidity, pressure and distance of the observations from the environment under consideration as the initial and/or boundary conditions of the diffusion equations developed from the remotely sensed data of the soil and groundwater. Experimental findings indicate that the model quantifies NO_2 concentrations with a precision of 10^{-6} g/m^3, attaining a minimal fitness value of 7.84×10^{-13} for soil and 3.73×10^{-11} for water. The reliability evaluation across 100 Monte Carlo simulations indicates a Global Mean Square Error (GMSE) of 4.32×10^{-4} and an NSE of 0.979 for soil, whereas for groundwater, the GMSE is 7.93×10^{-4} and the NSE is 0.935. Keeping in view reliability, convergence and computational complexity of the proposed scheme, it can be an effective alternative to analysis of soil and groundwater contamination in the laboratories.

Submitted 21 February 2025
Accepted 13 April 2026
Published 2 July 2026

Corresponding author
Eunchan Kim, eckim@hanyang.ac.kr

Academic editor
Consolato Sergi

Additional Information and Declarations can be found on page 18

DOI 10.7717/peerj-cs.3912

How to cite this article Ullah RS, Khan JA, Nasir IM, Kim E, Alsolai H, Allafi R, Arasi MA, Nafie FM. 2026. Neuro-deep fuzzy system for estimation of NO_2 concentration in soil and groundwater on highways from remote sensing images. **PeerJ Comput. Sci. 12:e3912**
DOI 10.7717/peerj-cs.3912

Subjects Algorithms and Analysis of Algorithms, Artificial Intelligence, Computer Vision, Data Mining and Machine Learning, Neural Networks
Keywords Fuzzy rules, Deep neural network, Remotely sensed soil parameters, Diffusion differential equation, NO_2 and nitric acid concentration, Monte Carlo simulations

INTRODUCTION

The remotely sensed images can be used to determine the earth observation through assessing the physical characteristics of an area in the form of large data with numerous attributes (*Liang, 2005*; *Bioucas-Dias et al., 2013*) that leads towards the valuable gains and decision makings. The actual benefits of the remote sensing (RS) data processing are observed in the hard area applications like polar sea ice monitoring, time series of ocean color (*Blondeau-Patissier et al., 2014*), fire management (*San-Miguel-Ayanz & Ravail, 2005*), hydrology and extremes (*Duan et al., 2021*) and coastal environmental change detections (*Alesheikh, Ghorbanali & Nouri, 2007*) *etc*. The real challenges of RS (*AghaKouchak et al., 2015*) are featuring interference, atmospheric conditions, transforming quantitative fact from the image features, data quality related issues, underexplored hard areas that can also be explored from Fig. S1. The natural merger of computer vision and RS data processing make the researcher capable enough to perform monitoring and prediction in the domain of agriculture (*Tian et al., 2020*), environment (*Donmez et al., 2021*), urban planning (*Ito & Biljecki, 2021*), building and road extraction and disaster management. The deep structurers, inherited parallelism, high-performance feature identification, accuracy and speed of deep learning models (*Basharat et al., 2023*) are made it viable to handle challenges (*Najafabadi et al., 2015*) like classify objects, features, detect change, data fusion, cloud removal, and spectral analysis in large RS image data.

The anthropogenic activities of mankind lead pollutants that causes various diseases and consequently effects the quality of life of living organism (*Khatri & Tyagi, 2015*). The core of all sources is that the harmful emissions of gases like nitrogen dioxide (NO_2), nitric acid and other range of injurious substances diffuse into the upper surface of soil and groundwater (*Leitgib, Kálmán & Gruiz, 2007*). The concentration of (NO_2) in soil is analyzed by considering as a local problem at each observation point on the surface with a single argument which is the distance of the observation points from the soil surface. A number of researchers contributes in the domain of RS and machine learning in the last two decades in various applications. In this regard a genetic algorithm (GA) based selective principal component analysis approach is applied for hyperspectral RS data in the domain of corn fields that reduces the bands of hyperspectral images upto 30% to 45% (*Chu et al., 2012*). The accuracy of proposed support vector machine (SVM) hybrid with GA (*Lin & Zhang, 2020*) outperforms in classifying the datasets of Landsat 5 TM, multidata dual polarization ALOS images and their textural information than that of stack-vector approach, however the computational complexity is given scheme is higher as compared to the single source data.

Recent studies have investigated deep learning models, including CNNs and hybrid architectures, for air quality prediction and soil contamination assessment.

Ghahremanloo et al. (2021) conducted a study that illustrated the effectiveness of deep convolutional neural networks (Deep-CNN) in estimating daily ground-level NO_2 concentrations, attaining a cross-validation R^2 of 0.91. This underscores the capability of deep learning methods to capture intricate spatial-temporal patterns of air pollution. Shirin et al. (2023) investigated the utilization of fuzzy and neural network models for monitoring environmental quality. The research highlighted the benefits of integrating fuzzy logic with neural networks to address uncertainties and nonlinearities in environmental data. Ekstrom & Hales (2000) presented a wavelet-based methodology for atmospheric pollution modeling, emphasizing the numerical integration of species-conservation equations. Their methodology successfully encompassed the multi-scale characteristics of pollution movement and dispersion. A recent study by He et al. (2025) established a hybrid wavelet-based deep learning model for precise air pollution forecasting. By utilizing wavelet transformations to decompose pollution data and integrating them into deep learning architectures, the model attained enhanced predictive accuracy relative to conventional methods. However, a number of modern research has been observed in the domain of RS data processing through tools of RS and modern form of artificial neural network (ANN) techniques like family of convolutional neural networks (CNNs), recurrent CNN (RCNN), shallow CNN (SCNN) *etc*. and cognitive based algorithms that assist the training of deep ANN models (Kattenborn et al., 2021). In this regards few contributions are worth mentioning like in Pang et al. (2024), the limitation of on-orbit computing in RS is addressed with Spiking neural networks (SNNs) that provide high speed and accuracy, biological plausibility, event-driven property and low power consumption. Moreover, Wang (2024) presented a modified firefly algorithm to get optimal structure of CNN for the segmentation of multispectral RS images with a better performance and accuracy.

Recent studies have advanced explainable AI in medical and agricultural imaging using deep learning and optimization techniques. Nasir et al. (2024a, 2024b) and Tehsin, Nasir & Damaševičius (2024) proposed attention-based and XGrad-CAM-enhanced models for interpreting CNN decisions in skin, breast, and brain cancer classification. In agriculture, Yousafzai et al. (2025a, 2025b) developed ensemble and transformer-based methods for wheat disease and head detection. Optimization frameworks were explored by Rajeena & Tehsin (2025) using Grey Wolf strategies, while Nasir et al. (2024a) and Malik et al. (2024) contributed to text categorization and secure image encryption. In document forensics, Tehsin et al. (2024) applied Siamese networks for signature verification. These works collectively highlight the growing synergy between explainability, deep learning, and optimization. A number of studies has been found in which successive layers of the deep neural network (DNN) are supported with fuzzy logic to create reliable decision where the data is incomplete or mathematical approximations are complex (Huang et al., 2024), explicitly speaking nonlinear system modeling through fuzzy neural networks. These fuzzy rules are used to infer an output based on input variables and are used now a days as an efficient computing tool, as a reference Takagi–Sugeno–Kang fuzzy system (Park & Lee, 2024) is exploited for deep interpretability of classification problems, the method has the capability of reducing the fuzzy rules as the reduction of parameters.

This study is significant as it addresses a gap by providing a remotely deployable, data-driven model that estimates NO_2 and nitric acid concentrations in soil and groundwater, which are critical markers of vehicular environmental impact. Our proposed method utilizes the universal approximation capacity of wavelet functions, the uncertainty modeling efficacy of fuzzy logic, and the convergence potential of particle swarm optimization-sequential quadratic programming (PSO-SQP) optimization to deliver an accurate and computationally economical substitute for physical sampling. The motivations behind fuzzy neural approach than that of Bayesian learning is the nature of input data that includes a mix of continuous sensor data, categorical/ordinal variables, and rule-based factors like boundary conditions. Another justification comes through the size of sample dataset that can be handled smoothly through neuro fuzzy models than that of transformer based models and Bayesian learning that requires large datasets to avoid overfitting.

The contributions of the presented work are as follows: The deep neural network modeling of the non-linear diffusion of contamination along with its initial and boundary conditions are performed in the form of unsupervised cost function in order to get soil response at any real point readily. To address the complex and continuous nature of RS data, a fuzzy layer is included in the hidden layer of DNN for local information extraction. The adaptive weights of the DNN are optimized with PSO hybrid with SQP based on trust region to manage deviation between the quadratic model and the actual target and use of L1-penalized subproblems to gradually decrease infeasibility. The Monte Carlo simulations are performed based on sufficiently large number of independent runs to guarantee the applicability of the proposed scheme, reliability, convergence and computational complexity in term of time.

The rest of the article is outlined in such a way that proposed methodology based on DNN modeling along with fuzzy rules hidden layer, creation of cost function based on the diffusion of contamination concentration and its initial and or boundary environmental conditions, logical steps implied for optimization of adaptive weights of DNN and key performance indicators are presented in 'Proposed Methodology'. In 'Results and Discussion', the scenario-based results and their discussion is presented while the conclusions are drawn in the last section.

PROPOSED METHODOLOGY

The proposed framework is designed in five phases; in the first phase deep neural network mathematical modeling is formulated based upon Mexican hat wavelet activation function, while the error function is generated in the form of mean square error (MSE) in the second phase. The inclusion of fuzzy layer in DNN based on optimistic formula is defined in the third phase while in the fourth phase mechanism of optimization schemes is provided to train the weights of the fuzzy deep neural network model. In the last phase last phase performance parameters are listed. Due to the nature of selected images for this study, no preprocessing is required to enhance the input images. The graphical workflow of the proposed methodology is presented in Fig. 1.

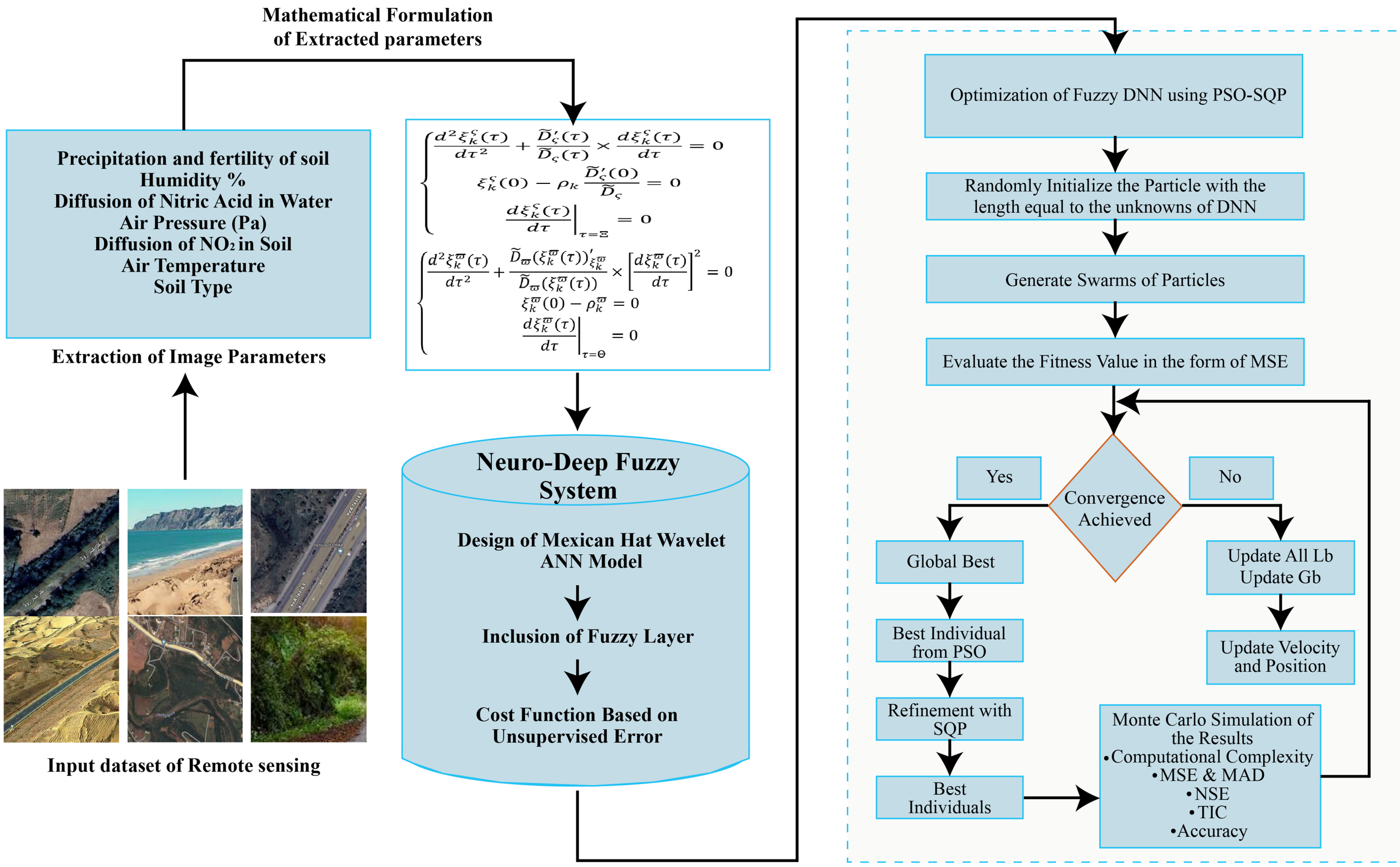

Figure 1 Graphical workflow of proposed methodology. Full-size DOI: 10.7717/peerj-cs.3912/fig-1

Data sources and acquisition

This work utilized environmental information obtained from the Sniffer4D air sensing platform, a portable multi-gas monitoring instrument capable of measuring NO_2 concentrations, ambient temperature, relative humidity, and atmospheric pressure. Measurements were performed in two distinct roadway environments: (1) urban/desert regions (Case-1) and (2) coastal/mountainous regions (Case-2). Each location was surveyed at different distances (0 to 200 m) and elevations (up to 200 m), emulating authentic mobile sensing conditions. The resultant data was archived in a structured CSV format, with each entry comprising spatial coordinates, timestamps, and sensor measurements. The datasets were utilized as boundary and initial condition inputs for the training, simulation, and validation of the fuzzy DNN framework. Data pre-processing was limited owing to the high resolution and real-time characteristics of the measurements.

Deep neural network modelling with fuzzy rules layer

The DNN modeling for the concentration of NO_2 in the soil and nitric acid in water as given in Eqs. (1) and (2) is performed as a continuous mapping of algebraic sum of

Mexican hat wavelet for the approximation of contamination and its first, second upto the nth derivative (*Wang & Qiao, 2021*), respectively, as:

$$\hat{\xi}(\tau) = \sum_{j=1}^{m} \left(\alpha_j \psi(w_j \tau + \beta_j) \right) \tag{1}$$

$$\frac{d^n \hat{\xi}}{d\tau^n} = \sum_{j=1}^{m} \alpha_j \frac{d^n}{d\tau^n} \psi(w_j \tau + \beta_j) \tag{2}$$

where α_j, w_j and β_j are the jth adaptive weights of the DNN, m is the number of neurons in the hidden layers and ψ is the Mexican hat wavelet activation/transfer function whose mathematical representation is given as *Siam et al. (2022)*:

$$\psi(\tau) = \frac{2}{\sqrt{3}} \pi^{-1/4} (1 - \tau^2) e^{-\tau^2/2}. \tag{3}$$

In Eq. (3), the constants 2 and 3 are integral elements of the normalized Mexican Hat (Ricker) wavelet function. These values are not particular to any variable; rather, they are incorporated to guarantee that the function possesses unit energy and maintains fundamental wavelet characteristics, like admissibility and a zero mean. By implying the transfer function in Eq. (3) for contamination in soil and water separately the obtained relationships are presented in the form of Eqs. (4) and (5), respectively.

$$\hat{\xi}^{\varsigma}(\tau) = \sum_{j=1}^{m} \alpha_j \left[\frac{2}{\sqrt{3}} \pi^{-0.25} \left(1 - (w_j \tau + \beta_j)^2 \right) e^{-0.5 (w_j \tau + \beta_j)^2} \right] \tag{4}$$

$$\hat{\xi}^{\varpi}(\tau) = \sum_{j=1}^{m} \beta_j \left[\frac{2}{\sqrt{3}} \pi^{-0.25} \left(1 - (w_j \tau + \alpha_j)^2 \right) e^{-0.5 (w_j \tau + \alpha_j)^2} \right]. \tag{5}$$

Moreover, the DNN modeling is extended upto the n^{th} order derivatives for better considerate.

$$\frac{d\hat{\xi}^{\varsigma}}{d\tau} = \sum_{j=1}^{m} \alpha_j \frac{d}{d\tau} \left[\frac{2}{\sqrt{3}} \pi^{-0.25} \left(1 - (w_j \tau + \beta_j)^2 \right) e^{-0.5 (w_j \tau + \beta_j)^2} \right] \tag{6}$$

$$\frac{d\hat{\xi}^{\varpi}}{d\tau} = \sum_{j=1}^{m} \beta_j \frac{d}{d\tau} \left[\frac{2}{\sqrt{3}} \pi^{-0.25} \left(1 - (w_j \tau + \alpha_j)^2 \right) e^{-0.5 (w_j \tau + \alpha_j)^2} \right]. \tag{7}$$

Creation of fitness evaluation function

The fitness evaluation function is generated in the form of residual error of the diffusion equation of the contaminated soil in Eq. (8) and water in Eq. (9) by mean of an unsupervised manner along with its error of initial and boundary conditions in Eq. (10) for the systems presented in Eqs. (1) and (2), respectively, the required error functions are obtained below:

$$\varepsilon_{\varsigma} = \frac{1}{T+1} \sum_{\tau=0}^{T} \left[\frac{d^2 \hat{\xi}_k^{\varsigma}(\tau)}{d\tau^2} + \frac{\tilde{D}_{\varsigma}{}'(\tau)}{\tilde{D}_{\varsigma}(\tau)} \cdot \frac{d\hat{\xi}_k^{\varsigma}(\tau)}{d\tau} \right]^2 \tag{8}$$

$$\varepsilon_{\varpi} = \frac{1}{T+1}\sum_{\tau=0}^{T}\left[\frac{d^2\hat{\xi}_k^{\varpi}(\tau)}{d\tau^2} + \frac{\tilde{D}_{\varpi}\left(\hat{\xi}_k^{\varpi}(\tau)\right)_{\left(\hat{\xi}_k^{\varpi}\right)'}}{\tilde{D}_{\varpi}\left(\hat{\xi}_k^{\varpi}(\tau)\right)}\cdot\left(\frac{d\hat{\xi}_k^{\varpi}(\tau)}{d\tau}\right)^2\right]^2. \tag{9}$$

Equations (8) and (9) denote the residual errors of the diffusion equations regulating NO_2 pollution in soil and groundwater, respectively. The residuals are calculated at various discretized intervals to measure the divergence of the DNN's predicted function from the actual physical model. They function as internal consistency verifications that guarantee the DNN approximation adheres to the fundamental partial differential equations.

$$\begin{aligned}\varepsilon_{\text{conditions}} = &\frac{1}{4}\left[\left(\hat{\xi}_k^{\varsigma}(0) - \rho_k\frac{\tilde{D}'_{\varsigma}(0)}{\tilde{D}_{\varsigma}(0)}\right)^2 + \left(\left.\frac{d\hat{\xi}_k^{\varsigma}(\tau)}{d\tau}\right|_{\tau=\Xi}\right)^2\right] \\ &+\frac{1}{4}\left[\left(\hat{\xi}_k^{\varpi}(0) - \rho_k^{\varpi}\right)^2 + \left(\left.\frac{d\hat{\xi}_k^{\varpi}(\tau)}{d\tau}\right|_{\tau=\Theta}\right)^2\right]\end{aligned}. \tag{10}$$

Equation (12) addresses inaccuracies in fulfilling the boundary and beginning conditions of the diffusion processes. This encompasses both the surface-level constraints (Dirichlet conditions) and the no-flux conditions at the lower boundaries (Neumann conditions). The comprehensive fitness function ε integrates the interior and boundary errors as an averaged squared metric. Reducing ε during training guarantees that the fuzzy DNN model complies with both the physical laws and the environmental restrictions of the problem area. Therefore,

$$\varepsilon = \left[\frac{1}{3}\left(\varepsilon_{\varsigma} + \varepsilon_{\varpi} + \varepsilon_{\text{conditions}}\right)^2\right]. \tag{11}$$

As $\varepsilon \to 0$, then at the same unknown weights of the fuzzy DNN, the functions converge such that:

$$\hat{\xi}^{\varsigma}(\tau) \to \xi^{\varsigma}(\tau) \quad \text{and} \quad \hat{\xi}^{\varpi}(\tau) \to \xi^{\varpi}(\tau). \tag{12}$$

Inclusion of fuzzy layer in DNN

The fuzzy rule is encompassed in such a way that each hidden layer of DNN is strengthened with an additional layer of fuzzy that determines the parameter estimation using the optimistic formula (*Jeong et al., 2022*) of fuzzy rules. The mathematical description of the fuzzy layer is defined below:

$$\begin{aligned}&\langle\tau_1, \tau_2, \ldots, \tau_m\rangle, \left\{\langle\xi_1^i, \xi_2^i, \ldots, \xi_m^i\rangle \mid 1 \le i \le \delta\right\} \\ &\qquad\left\{\langle w_{j,1}^i, w_{j,2}^i, \ldots, w_{j,m_{i+1}}^i\rangle \mid 1 \le j \le m_i\right\}, \left\{\langle\beta_1^i, \beta_2^i, \ldots, \beta_{m_i}^i\rangle\right\}\end{aligned}. \tag{13}$$

The optimistic formula of fuzzy rule exploited is given below in Eq. (13).

$$w \times \tau = \langle\mu_{w\tau}, \nu_{w\tau}\rangle = \langle\max(\mu_w, \mu_\tau), \min(\nu_w, \nu_\tau)\rangle, \quad \mu_\tau \text{ and } \nu_\tau \in [0, 1]. \tag{14}$$

Equation (13) delineates the fuzzy multiplication operation $w \times \tau$ within the framework of interval-valued fuzzy logic, wherein the membership function is articulated as a pair

(μ, v), signifying the lower and upper limits of belief. In this context, the 'optimistic' technique presumes the most favorable outcome: the highest lower bounds for membership (denoting strong conviction) and the lowest upper bounds for non-membership (signifying less ambiguity). This method is especially appropriate for noisy or inaccurate input data, as found in remote sensing applications.

This operation merges two interval-valued fuzzy sets, each characterized by a membership degree μ and a non-membership degree (or upper bound) v, in an optimistic manner. It specifically identifies the maximum belief (*i.e.*, the more compelling of the two supporting evidences) and the minimum disbelief (*i.e.*, the least contradictory evidence). This optimistic principle guarantees that when integrating imprecise or uncertain input, such as that obtained from remote sensing, the inference prioritizes stronger evidence, resulting in more definitive outcomes and so improving the interpretability and resilience of the network amidst uncertainty. The proposed fuzzy system has fuzzy rules, generated by the combination of input linguistic variables that contain overall thirteen rules. The Gaussian membership function is exploited with optimistic inference strategy and standard Takagi–Sugeno rule formulation to integrate both linguistic antecedents and numeric consequents.

Optimization of the weights of DNN model

The unknown real valued weights of the DNN model have been tuned by PSO as a global optimizer hybrid with SQP as a local search technique called PSO-SQP. In brief, PSO is employed first to perform global exploration and identify a promising region of the search space. Once the PSO iterations converge to a near-optimal region determined by either stagnation of swarm best fitness or achieving the predefined tolerance threshold. SQP is then activated as a local refinement stage whose input is the final best vector (unknown) of PSO. The mutual strength of both the algorithms not only ensure the optimized weights for DNN but also avoid the pre-mature convergence as well whose logical steps are presented below:

Step 1: Initialization of the particles: Create a primary swarm as a set of arbitrarily dispersed particles using constrained real values. The length of each particle is equivalent to the adaptive weights of the DNN model and is considered as a candidate solution.

Step 2: Formulation of cost function: The cost function is represented as ε and is determined in the form of MSE with the help of Eq. (13) followed by Eqs. (10) to (12). The fitness value is calculated for each unknown while the velocity and position of the unknown is updated by using the standard equations of the PSO algorithm available in the literature (*Marini & Walczak, 2015*).

Step 3: Exit criteria: The execution of PSO will be terminated if predefined fitness value achieved, maximum number of iterations are executed, if the value of the global best does not change for 10 iterations, function tolerance = 10^{-12}

If termination criteria are met, then go to step 6 else continue. The function tolerance is established at 10^{-12} to guarantee high-precision convergence of the optimization process,

Table 1 Hyperparameter values/setting for PSO and SQP.

PSO		SQP	
Parameters	Setting	Parameters	Setting
Swarm size	200	Start point	Best weights of PSO
Particle length	30	Derivative	Solver approximate
Flights	500	Iterations	100
C_1	1.75	Max function evaluation	100,000
C_2	1.5	Finite difference type	Central difference
Bounds	Lb = −10, Ub = 10	Bounds	Lb = −10, Ub = 10
ω	[0.9 to 0.4]	Hessian	BFGS
V_{max}	4.0	Minimum perturbation	10^{-08}
Population span	[−15 to 15]	x-tolerance	10^{-25}
Velocity span	[−4 to 4]	Nonlinear function tolerance	10^{-25}
Others	Default	Others	Default

as the cost function μ denotes minor residuals obtained from physical diffusion equations. A more stringent criterion is crucial to achieve the precise precision necessary for simulating actual contamination levels, particularly when target fitness values vary from 10^{-11} to 10^{-13}.

Step 4: Ranking: Updated the global and local best particles of the swarm and ranked them according to the maximum fitness by performing the index sort.

Step 5: Renewal of particle by updating the velocity and position: Updated velocity and position of the particles using the standard equations of PSO and repeat steps 2 to 5 until the total number of flights is completed.

Step 6: Enhancement of weights tuning using SQP: The fine-tuning of the results obtained from the PSO is performed using SQP, in this regard the best particles obtained from PSO as a global optimizer are passed as a start point to the local optimizer called SQP, the detailed parameter values/setting used both the algorithms are tabulated in Table 1.

Step 7: Data storage, analysis and Monte Carlo simulations: Store the weights of the best particle, best fitness values and execution Time. For reliability, repeat steps 1 to 6 for a large number of independent runs and perform the analysis.

RESULTS AND DISCUSSION

In this section two case studies have been taken systematically with reference to the nature of the environment and parametric characteristics; one the highways along the side of the deserts, dry areas and city zone while in the second case study deals with the highways at the sides of the sea, mountains or water sources like lakes. The simulations are performed on the hardware with the specifications Intel (R) Core (TM) i7-8550U CPU @1.99 GHz with 16.0 GB RAM while software used is MATLAB® R2023b.

The hyperparameters values/settings of the PSO-SQP algorithm are adjusted after a chamber some process that leads the neuro fuzzy DNN system towards an effective and reliable computing tool, best parameters values used in the whole simulations are presented in Table 1. To assess the resilience and flexibility of the proposed neuro-deep fuzzy system, we establish two experimental scenarios: Case-1 and Case-2. These cases are chosen to exemplify diverse environmental contexts and contamination routes. Case-1 examines soil contamination by NO_2 resulting from heavy traffic on highways in arid regions, deserts, and metropolitan areas where soil surface interaction prevails. Conversely, Case-2 addresses groundwater pollution from nitric acid near roadways close to aquatic environments including lakes, coastal regions, and hilly locations, where subsurface water percolation is more pronounced. The selected settings were intended to represent distinct conditions, pollution dynamics, and monitoring issues, facilitating the validation of our model's generalizability across diverse real-world scenarios.

Case-1

The assessment of NO_2 on soil contamination has been executed on the highways in the 200 m of the city zone, desert or dry areas. The sections of the highway taken under consideration is characterized by the busy heavy traffic. The measurements have been executed at a vertical height 2–200 m from the surface layer above the road and along the road at a distance of [2–50] m. Sniffer4D (*Botella et al., 2004*) is used to sense the pollution sources on the above-mentioned highways and calculate the parametric values of the ρ_k, Ξ and parameters of the air conditions to find out the values of the initial conditions and parameters for the system given in Eq. (1). These obtained values are transmitted to the workstations for Fuzzy DNN modeling and processing to get useful decisions. In this regard the depth of the soil is taken as $\tau \in [0, 0.14]$ meter with a step size of 0.02. The values of the random adaptive weights vector $[\alpha\, w\, \beta]_{1\times 30}$ of the DNN are taken from [−10 to 10]. After applying the PSO-SQP algorithm on fuzzy DNN the results of the weights are plotted in Fig. S2, which illustrates the adaptive weights of the fuzzy DNN subsequent to optimization *via* PSO-SQP. The weights vary from −10 to 10, indicating the refinement accomplished by the hybrid optimizer. The erratic yet confined pattern signifies that the network has effectively settled on a solution that harmonizes generalization with constraint satisfaction, facilitating precise modeling of NO_2 diffusion in soil under specified environmental circumstances. By putting these unknown weights in the Eqs. (10) to (12), the fitness value (f_{val}) is obtained from the range 10–12 to $10 - 13$ for snapshots at a distance of 0, 40, 80, 120, 160 and 200 m, respectively from the surface of earth and eventually concentrations of NO_2 in $10^{-06}\ g/m^3$. The results of the proposed methodology that satisfies the condition $\hat{\xi}^{\varsigma}(\tau) \to \xi^{\varsigma}(\tau)$ on the obtained weights are tabulated in Table 2.

The model's compliance with this physical boundary behavior confirms the efficacy of the fuzzy-enhanced wavelet DNN in simulating shallow subsurface pollution. The figure is drawn at log scale to clearly explain the difference of variation of the concentration of NO_2 with the change in depth. It is evident that the contamination lies only up to a depth of 0.1 m, with the highest level at $\tau = 0$. Figure S3 shows the behavior of contamination with soil depth.

Table 2 NO_2 measured values for Case-1.

Case 1	Distance (m)	Air temperature (C^0)	Air humidity %	Air pressure (mm of Hg)	Concentration of NO_2 10^{-06} g/m^3
Road-a	0	22.14	66.3	702.0	14.261
	40	22.65	67.1	702.2	14.672
	80	22.71	66.9	702.8	14.724
	120	22.35	66.9	702.4	14.822
	160	22.59	66.8	702.3	13.890
	200	22.83	67.0	702.4	13.933
Road-b	0	23.12	59.0	698.2	10.344
	40	23.73	59.2	689.8	10.123
	80	24.72	59.1	689.4	10.216
	120	23.53	59.2	689.1	10.118
	160	23.02	59.0	689.3	10.242
	200	23.87	59.2	689.7	10.168
Road-c	0	21.12	80	712.2	12.645
	40	21.56	80	711.2	12.534
	80	21.42	82	711.4	12.485
	120	21.76	82	712.2	12.475
	160	21.12	82	712.6	12.967
	200	21.61	82	711.2	12.673

It can be concluded from the table that a contamination of NO_2 from 13.890 to 14.822 μg/m^3, 10.118 to 10.344 μg/m^3 and 12.475 to 12.967 μg/m^3 is observed at a specified air conditions in term of temperature, pressure and humidity for data set. It is worth mentioning that this concentration of contaminations was at the top most layer of soil. However, the detail analysis for this is also performed by considering the depth of the soil from 0 to 0.14 m in order to have close analysis. The results for the surface contamination $\rho = 35.65,\ 41.5,\ \text{and}\ 42.7$, respectively. These values correspond to surface NO_2 concentrations captured by Sniffer4D sensor units deployed at different highway zones, representing diverse urban and dry area scenarios. The raw concentration readings were filtered using a moving error window to remove noise and transient spikes caused by the external sources. The time average concentration is used for getting robust boundary conditions, based upon predefined variance threshold. They serve as initial boundary conditions for solving the diffusion equation in Eq. (1). A logarithmic scale is employed to represent the steep gradient near the surface. The swift decline beyond 0.1 m indicates that the majority of pollutant diffusion is confined to the higher soil strata. The model's compliance with this physical boundary behavior confirms the efficacy of the fuzzy-enhanced wavelet DNN in simulating shallow subsurface pollution.

The figure is drawn at log scale to clearly explain the difference of variation of the concentration of NO_2 with the change in the depth, it is quite evident that the contamination lies only upto the depth of 0.1 m only with this fact that its highest level is at $\tau = 0$. Moreover, in order to have a closer look on the behavior of concentration of NO_2 with the soil depth the matrices of records are stored for observation points with varying perpendicular distances [0 to 250 m] whose graphical representation is presented in Fig. S4, which illustrates the fluctuation of NO_2 deposits in relation to vertical height above ground level at several observation stations. The minor variations at each depth layer indicate that although air exposure fluctuates slightly with elevation, the concentration at the surface level stays predominant. This spatial consistency emphasizes the model's stability across vertical observations and endorses its use in mobile aerial monitoring systems. It can be observed that for any specific depth of the soil there is a small variation in concentration of NO_2 deposited at observation points examined from different vertical heights.

Case-2

The assessment of nitric acid in the underground water due to exhaust of the vehicles on the highways are examined on the same hyperparameter values as given in Table 1 by considering the vertical height from 0 to 160 m vertical height from the water source, sea side and mountain area. The average depth of the contaminated water is taken as $\tau \in [0, 0.14]$ m with a step size of 0.02 due to the irregular patches. Sniffer4D is used to sense the pollution sources and calculate the parametric values of the ρ_k and Θ to find out the values of the initial conditions of the system given in Eq. (2). After applying the proposed technique, the optimized adaptive variables tuned by PSO-SQP algorithm for the system given in Eq. (2) are presented in the form of 3D graph in Fig. S5, which illustrates the optimum weight distribution for groundwater contamination modeling employing the identical PSO-SQP approach. The more uniform and marginally tighter distribution illustrates the consistent character of waterbody diffusion relative to soil, as water functions as a continuous medium with diminished material heterogeneity.

The one of the best optimized variable vectors is observed to be in the range from -10 to 10 as shown in the Fig. S6. The cost function achieved by the proposed approach is 3.732×10^{-11} for the specific values of the weights. However, if we observed the cost function by varying the vertical heights of the observation from 0 to 160 m the value of the fitness (f_{val}) is found to be in the range 10^{-11} to 10^{-12}. Moreover, the concentration of contamination of nitric acid is approximated on the optimized weights by following the condition as $\hat{\xi}^{\varpi}(\tau) \rightarrow \xi^{\varpi}(\tau)$ whose results are tabulated in Table 3 while the behavior of nitric acid concentration with the depth of the water source is presented in Fig. S6 at different values of the $\rho = 34.23,\ 35.72,$ and 36.79, respectively. These values were obtained through Sniffer4D measurements at coastal, lake-adjacent, and mountainous highway sites and represent surface-level concentrations of nitric acid in water used as Dirichlet conditions for Eq. (2). Figure S6 illustrates the reduction of nitric acid concentration with increasing water depth. Analogous to the soil scenario, contamination predominantly resides within the upper 0.1 m; however, the gradient is less pronounced owing to the solubility and mixing characteristics of water. The fuzzy DNN accurately represents this transition, conforming to theoretical predictions for shallow waterbody diffusion.

Moreover, in order to have better evidence on the behavior of concentration of nitric acid with the underground water depth the matrices of records are stored for observation points with varying perpendicular distances [0 to 120 m] whose graphical representation is

Table 3 Concentration of nitric acid measured for case-2.

Case 2	Distance (m)	Air temperature C^0	Air humidity %	Air pressure (mm of Hg)	Concentration of NO_2 10^{-06} g/m^3
Road-a	0	23.02	45	712.3	13.012
	40	23.40	46	713.2	12.982
	80	22.91	45	712.9	13.210
	120	23.12	45	713.2	12.109
	160	23.12	44	712.9	12.912
Road-b	0	26.71	37	758.9	12.761
	40	27.03	38	759.3	12.942
	80	27.38	37	758.8	12.362
	120	27.81	37	759.7	12.129
	160	27.49	38	759.2	12.821
Road-c	0	20.12	62	758.3	10.092
	40	20.34	61	760.1	9.9820
	80	20.71	62	759.8	10.089
	120	20.16	62	758.4	10.118
	160	20.19	61	758.7	10.242

presented in Fig. S7 which examines the concentration of nitric acid at different vertical elevations from the sea surface. Although slight change is observed within the 0–120 m range, the overarching trend indicates stability in the distribution of spatial concentration. This outcome corroborates the hypothesis that once contaminants infiltrate the waterbody, their lateral dispersion becomes uniform, hence justifying the use of vertically dispersed sensors for effective monitoring. It can be observed that for any specific average depth of the water there is a small variation in concentration of NO_2 deposited at observation points examined from different vertical heights.

In contrast to current deep learning models for air quality estimation, such as CNN-based regression frameworks (*Ghahremanloo et al., 2021*), our proposed neuro-deep fuzzy system provides a distinctive equilibrium between physical interpretability and computational efficiency. Unlike most previous models that depend predominantly on supervised learning with labeled pollution datasets, our methodology is unsupervised and governed by differential equations, allowing for adaptability to novel situations without the need for retraining. Furthermore, the incorporation of a fuzzy logic layer augments the model's robustness against ambiguous or erratic sensor inputs—a significant drawback in traditional deep learning models. Fuzzy neural systems have demonstrated efficacy in environmental monitoring (*Carnevale et al., 2009*), and we enhance this by integrating fuzzy logic into the framework of a wavelet-based deep neural network trained using PSO-SQP, guaranteeing smooth convergence and precision under varied situations. The model's principal strength is its modular architecture: the wavelet layer approximates nonlinear diffusion, the fuzzy layer translates ambiguous observations, and the PSO-SQP hybrid guarantees effective optimization.

The reliable solution of the given framework is observed in Fig. 2A for both of cases, it is quite clear from the graph that overall MSE of Case-1 is better than that of the Case-2 for

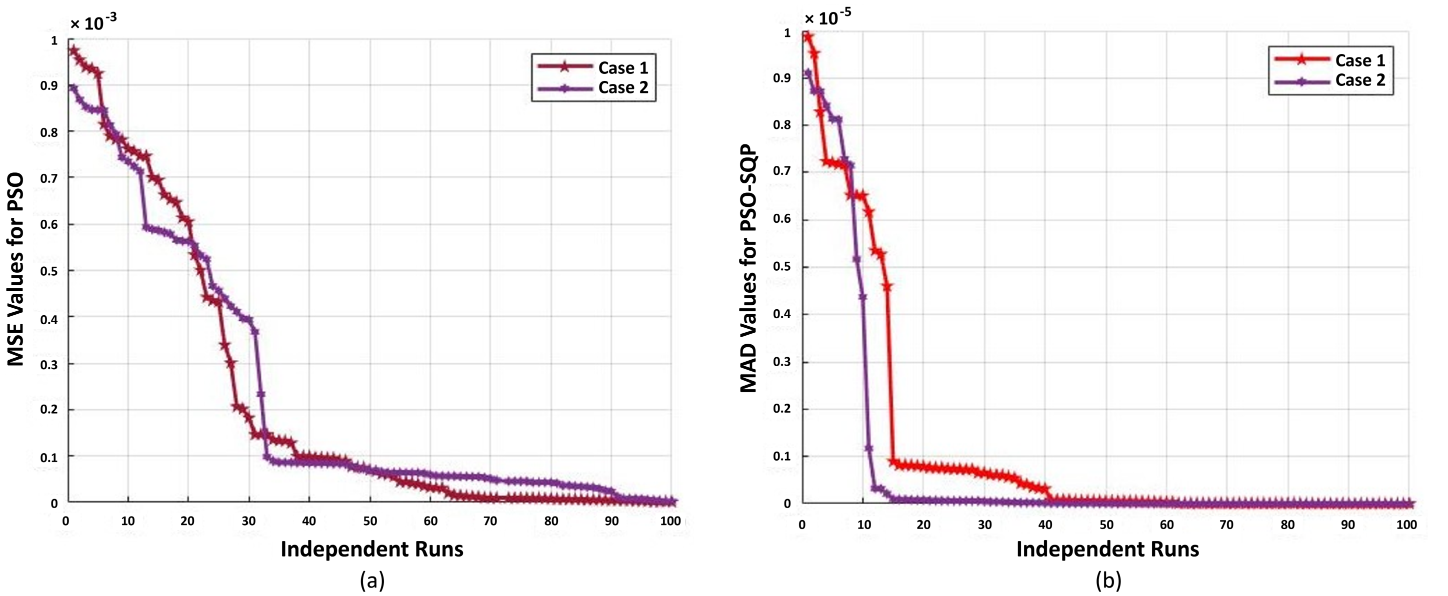

Figure 2 (A and B) Comparison of results for Case-1 and Case-2. Full-size DOI: 10.7717/peerj-cs.3912/fig-2

Table 4 Performance analysis of Fuzzy-DNN approach.

Case study	GMSE	GMAD	GMET (sec)	NSE
Case-1	4.321×10^{-4}	3.678×10^{-4}	132.23	0.979
Case-2	7.935×10^{-4}	2.354×10^{-4}	140.28	0.935

Note:
Global Mean Square Error (GMSE), Global Mean Absolute Deviation (GMAD), Global Mean Execution Time (GMET), Nash–Sutcliffe Efficiency (NSE).

most of the 100 independent runs. However, the convergence of the both the cases are presented in Fig. 2B in the form of GMAD. Keeping in view the value of Nash–Sutcliffe Efficiency (NSE) for both of the cases, it can be concluded that the model based on fuzzy DNN is a perfect model with an estimation error variance equal to zero. Table 4 shows the performance analysis of fuzzy DNN approach.

COMPARISON WITH STATE OF ART EXISTED TECHNIQUES

The results of the proposed Fuzzy-DNN are compared with the BYADNN model of *Casolaro, Capone & Camastra (2025)*, PatchTST by *Casolaro et al. (2023)*, and the RFR-ConGRU model presented by *Mudassar et al. (2026)*; these results are tabulated in Table 5. The comparison is carried out using several evaluation metrics, including Global Root Mean Square Error (GRMSE), Global Fitness Value (Fit-Val), Giga Floating Point Operations Per Second (GFLOPs), and Cohen's Kappa (κ). These measures evaluate the prediction accuracy, computational efficiency, and classification reliability of the models. From the table, the GRMSE value of the proposed model is 0.037, which is significantly lower than the BYADNN (2.561), PatchTST (0.234), and RFR-ConGRU (14.571) models. Since a lower GRMSE indicates smaller prediction error, this result demonstrates that the

Table 5 Performance comparison with state of art existed techniques.

Performance measure	BYADNN model	Patch TST	RFR-ConGRU	Proposed
GRMSE	2.561	0.234	14.571	0.037
Global Fit-Val	2.100E−03	2.520E−02	8.230E−02	3.000E−04
Global Com-Cost (GFLOPs)	0.3246	0.6865	0.8276	0.2394
Cohen's kappa	0.852	0.787	0.671	0.914

proposed Fuzzy-DNN model provides much more accurate predictions than the existing techniques. Similarly, the Global Fit-Value, which measures the closeness of the model output to the true observations, is 3.0×10^{-4} for the proposed model. This value is considerably smaller than those of the other models (2.1×10^{-3}, 2.52×10^{-2}, and 8.23×10^{-2}), indicating that the proposed approach achieves a much better global optimization performance.

In terms of computational complexity measured by GFLOPs, the proposed model requires 0.2394 GFLOPs, which is lower than BYADNN (0.3246), PatchTST (0.6865), and RFR-ConGRU (0.8276). This shows that the proposed Fuzzy-DNN architecture is computationally more efficient and requires fewer floating-point operations during model execution, making it suitable for real-time or resource-constrained environments. Finally, the Cohen's Kappa coefficient further validates the superiority of the proposed model. The proposed model achieves a κ-value of 0.914, which represents almost perfect agreement between predicted and actual outcomes. In comparison, the κ values of BYADNN (0.852), PatchTST (0.787), and RFR-ConGRU (0.671) indicate comparatively lower agreement levels.

From the table, the GRMSE value of the proposed model is 0.037, which is significantly lower than the BYADNN (2.561), PatchTST (0.234), and RFR-ConGRU (14.571) models. Since a lower GRMSE indicates a smaller prediction error, this result demonstrates that the proposed Fuzzy-DNN model provides much more accurate predictions than the existing techniques. Similarly, the Global Fit-Value, which measures the closeness of the model output to the true observations, is 3.0×10^{-4} for the proposed model. This value is considerably smaller than those of the other models (2.1×10^{-3}, 2.52×10^{-2}, and 8.23×10^{-2}), indicating that the proposed approach achieves a much better global optimization performance. In terms of computational complexity measured by GFLOPs, the proposed model requires 0.2394 GFLOPs, which is lower than BYADNN (0.3246), PatchTST (0.6865), and RFR-ConGRU (0.8276). This shows that the proposed Fuzzy-DNN architecture is computationally more efficient and requires fewer floating-point operations during model execution, making it suitable for real-time or resource-constrained environments. The proposed model achieves a κ-value of 0.914, which represents almost perfect agreement between predicted and actual outcomes. In comparison, the κ values of BYADNN (0.852), PatchTST (0.787), and RFR-ConGRU (0.671) indicate comparatively lower agreement levels.

The RMSE of the proposed model with the existing state-of-the-art models over 10 different instances are illustrated in Fig. 3. The PatchTST model, the RFR-ConGRU Model,

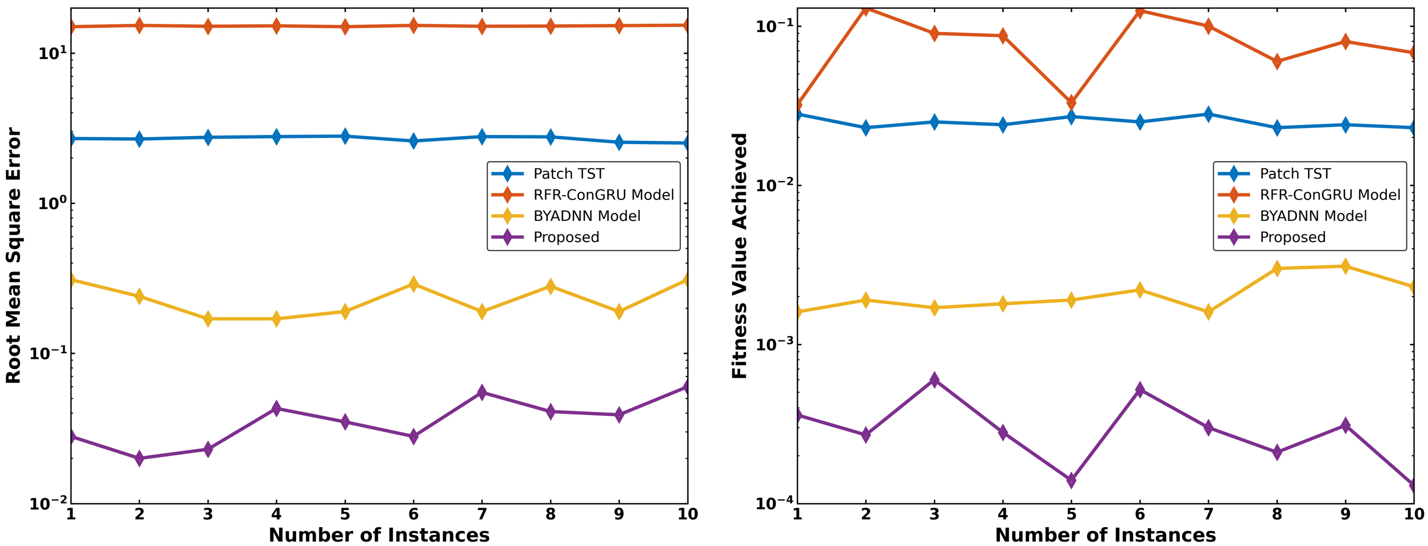

Figure 3 **Comparison of proposed Fuzzy-DNN with state-of-the-art techniques.** Full-size DOI: 10.7717/peerj-cs.3912/fig-3

the BYADNN Model, and the proposed Fuzzy-DNN Model are compared by taking number of instances on the x-axis, while the y-axis represents the corresponding RMSE values on the logarithmic scale. In this figure, it can be clearly identified that the RFR-ConGRU Model performs with the highest values of RMSE, which represents the highest errors. The PatchTST model performs with moderate values of RMSE. The BYADNN Model performs better than the PatchTST Model with lower values of RMSE, around 10^{-1}. However, the proposed Fuzzy-DNN Model performs with the minimum values of RMSE, around 10^{-2} to 10^{-1}.

The comparative analysis based on the fitness value results achieved through 10 different instances for four different models: PatchTST model, RFR-ConGRU model, BYADNN model, and the proposed Fuzzy-DNN model are plotted in Fig. S8 on the logarithmic scale. It is quite evident from the Figure that the RFR-ConGRU Model has achieved the highest fitness value results that leads towards the lowest accuracy, which indicates that it has performed poorly in optimization results compared to other models. The PatchTST model has achieved moderate fitness value results compared to other models. The BYADNN model has achieved lower fitness value results compared to other models but has achieved varying results in each instance.

The results of the computational complexity achieved in term of GFLOPs is presented in Fig. S8, it is quite evident from the figure that the proposed model has the least computational complexity, ranging between 0.2008 and 0.2773 GFLOPs, with a mean of 0.2394 ± 0.0298 GFLOPs. The proposed model is therefore not only accurate but also computationally efficient, as can be seen when comparing with other models: BYADNN requires 0.3246 ± 0.0189 GFLOPs, PatchTST requires 0.6865 ± 0.0619 GFLOPs, while RFR-ConGRU requires 0.8276 ± 0.0865 GFLOPs.

Table 6 shows a statistical performance analysis of four different deep learning models for 10 different experimental runs. Here, the models used for comparison are BYADNN

Table 6 Statistical analysis of various performance measures with state of art existed techniques.

Performance measure	Statistical mode	BYADNN model	Patch TST	RFR-ConGRU model	Proposed
RMSE	MIN	2.317	0.172	14.224	0.019
	MAX	2.731	0.307	14.960	0.060
	μ	2.561	0.234	14.571	0.037
	σ	0.153	0.056	0.255	0.014
	$\mu \pm \sigma$	2.561 ± 0.153	0.234 ± 0.056	14.571 ± 0.255	0.037 ± 0.014
	p-value	0.0151	0.0098	0.0471	0.0017
Fit-Val	MIN	1.600×10^{-3}	2.290×10^{-2}	3.250×10^{-2}	1.000×10^{-4}
	MAX	3.000×10^{-3}	1.322×10^{-1}	2.830×10^{-2}	6.000×10^{-4}
	μ	2.100×10^{-3}	2.520×10^{-2}	8.230×10^{-2}	3.000×10^{-4}
	σ	5.000×10^{-4}	3.440×10^{-2}	2.000×10^{-3}	1.000×10^{-4}
	$\mu \pm \sigma$	$(2.100 \pm 0.500) \times 10^{-3}$	$(2.520 \pm 3.440) \times 10^{-2}$	$(8.230 \pm 0.200) \times 10^{-2}$	$(3.00 \pm 1.00) \times 10^{-4}$
	p-value	0.0147	0.0035	0.0327	0.0012
Com-Cost (GFLOPs)	MIN	0.3099	0.6155	0.7222	0.2008
	MAX	0.3632	0.7828	0.9964	0.2773
	μ	0.3246	0.6865	0.8276	0.2394
	σ	0.0189	0.0619	0.0865	0.0298
	$\mu \pm \sigma$	0.3246 ± 0.0189	0.6865 ± 0.0619	0.8276 ± 0.0865	0.2394 ± 0.0298
	p-value	0.0149	0.0078	0.0328	0.0019

Model, PatchTST Model, RFR-ConGRU Model, and the Proposed Fuzzy Deep Neural Network model. In the evaluation process, different statistical measures such as minimum (MIN), maximum (MAX), mean (μ), standard deviation (σ), mean $\pm$ standard deviation ($\mu \pm \sigma$), and 'p' values are taken into consideration for different performance measures. For the Root Mean Square Error (RMSE) measure, where error in prediction is concerned, the best minimum value for the Proposed model is 0.019, and the maximum value is 0.060. Also, the mean value for the Proposed model is 0.037 ± 0.014, which is much lower compared to the values obtained for BYADNN (2.561 ± 0.153), PatchTST (0.234 ± 0.056), and RFR-ConGRU (14.571 ± 0.255).

In the case of the Fit-Value, where the prediction output is measured against the actual output, the proposed model has again performed better than the existing models. In the 10 different instances, the proposed model has shown a range from 1.0×10^{-4} to 6.0×10^{-4}, with a mean value of $3.0 \times 10^{-4} \pm 1.0 \times 10^{-4}$. The existing models are found to have higher mean values, such as BYADNN, where the value is $2.100 \times 10^{-3} \pm 5.000 \times 10^{-4}$, PatchTST, where the value is $2.520 \times 10^{-2} \pm 3.440 \times 10^{-2}$, and RFR-ConGRU, where the value is $8.230 \times 10^{-2} \pm 2.000 \times 10^{-3}$.

CONCLUSION

This study introduced a hybrid neuro-deep fuzzy framework that utilizes a wavelet-based deep neural network, augmented with fuzzy logic and optimized *via* a PSO-SQP mechanism, to model NO_2 pollution in soil and groundwater adjacent to highways. The model was engineered to function autonomously, regulated by physical diffusion principles, and configured to integrate environmental variability through remote sensing data. The suggested system incorporates a fuzzy logic layer with a wavelet-based activation mechanism, providing a novel approach that improves interpretability, addresses uncertainty, and generalizes across various environmental contexts. The framework's amalgamation of neural approximation, fuzzy rule reasoning, and hybrid optimization renders it a formidable contender for non-invasive environmental monitoring systems. This methodology, while primarily focused on vehicular pollution modeling, can be extended for various environmental concerns that require data-driven physical estimation. This study enhances the expanding *corpus* of research at the convergence of artificial intelligence, environmental modeling, and remote sensing technology.

The limitation of this work is that it solely depends on initial condition as diffusion equations are depends on the environmental conditions, thus the results and concentration of NO_2 will change on every execution. Therefore, a hardware-based robust model should monitor the amount of these concentrations. In future, one may investigate the other contamination, available due to the exhaust of vehicles and effects of the contamination due to other sources and its effects on the fertility of soil for the domain of agriculture and other allied fields. Moreover, the architectures, based on Transformer learning, EfficientNet, and Attention Based models can be exploited to see the concentration level of NO_2 and other contaminations in soil. Another future direction can be to explore Bayesian neural fuzzy models to see the air quality forecasting. and its allied domains.

ADDITIONAL INFORMATION AND DECLARATIONS

Funding

This research was supported by the research fund of Hanyang University (HY-202400000003701), the Deanship of Research and Graduate Studies at King Khalid University through the Large Research Project under grant number RGP2/219/46, Princess Nourah bint Abdulrahman University Researchers Supporting Project number (PNURSP2026R303), Princess Nourah bint Abdulrahman University, Riyadh, Saudi Arabia, the Deanship of Scientific Research at Northern Border University, Arar, KSA through the project number "NBU-FFR-2026-1516-04, and by the Deanship of Scientific Research at Majmaah University under Project No. FR-2026-151. The Hanyang University, King Khalid University, Princess Nourah bint Abdulrahman University, Northern Border University, and Majmaah University had contributed to the study design, data collection, and analysis; however, they had no role in the decision to publish or in the preparation of the manuscript.

Grant Disclosures

The following grant information was disclosed by the authors:
Hanyang University: HY-202400000003701.
Deanship of Research and Graduate Studies at King Khalid University.
Large Research Project: RGP2/219/46.
Princess Nourah bint Abdulrahman University Researchers, Riyadh, Saudi Arabia:

PNURSP2026R303.
Deanship of Scientific Research at Northern Border University, Arar, KSA: NBU-FFR-2026-1516-04.
Deanship of Scientific Research at Majmaah University: FR-2026-151.

Competing Interests

The authors declare that they have no competing interests.

Author Contributions

- Raja Shamayel Ullah conceived and designed the experiments, analyzed the data, prepared figures and/or tables, and approved the final draft.
- Junaid Ali Khan conceived and designed the experiments, analyzed the data, prepared figures and/or tables, supervision, and approved the final draft.
- Inzamam Mashood Nasir conceived and designed the experiments, performed the computation work, prepared figures and/or tables, supervision, and approved the final draft.
- Eunchan Kim conceived and designed the experiments, performed the experiments, analyzed the data, prepared figures and/or tables, project administration, and approved the final draft.
- Hadeel Alsolai performed the experiments, authored or reviewed drafts of the article, and approved the final draft.
- Randa Allafi performed the experiments, authored or reviewed drafts of the article, and approved the final draft.
- Munya A. Arasi performed the experiments, authored or reviewed drafts of the article, and approved the final draft.
- Faisal Mohammed Nafie performed the experiments, authored or reviewed drafts of the article, and approved the final draft.

Data Availability

The following information was supplied regarding data availability:

The code is available at GitHub and Zenodo:

- https://github.com/imashoodnasir/Neuro-Deep-Fuzzy-System.

- Nasir, I. M. (2025). Neuro-Deep-Fuzzy-System. https://doi.org/10.5281/zenodo.15475988.

All simulations are performed on the images located in Fig. S1.

Supplemental Information

Supplemental information for this article can be found online at http://dx.doi.org/10.7717/peerj-cs.3912#supplemental-information.

REFERENCES

AghaKouchak A, Farahmand A, Melton FS, Teixeira J, Anderson MC, Wardlow BD, Hain CR. 2015. Remote sensing of drought: progress, challenges and opportunities. *Reviews of Geophysics* **53(2)**:452–480 DOI 10.1002/2014rg000456.

Alesheikh AA, Ghorbanali A, Nouri N. 2007. Coastline change detection using remote sensing. *International Journal of Environmental Science & Technology* **4(1)**:61–66 DOI 10.1007/bf03325962.

Basharat Mu, Khan JA, Abdo HG, Almohamad H. 2023. An integrated approach based landslide susceptibility mapping: case of Muzaffarabad region, Pakistan. *Geomatics, Natural Hazards and Risk* **14(1)**:2210255 DOI 10.1080/19475705.2023.2210255.

Bioucas-Dias JM, Plaza A, Camps-Valls G, Scheunders P, Nasrabadi N, Chanussot J. 2013. Hyperspectral remote sensing data analysis and future challenges. *IEEE Geoscience and Remote Sensing Magazine* **1(2)**:6–36 DOI 10.1109/mgrs.2013.2244672.

Blondeau-Patissier D, Gower JFR, Dekker AG, Phinn SR, Brando VE. 2014. A review of ocean color remote sensing methods and statistical techniques for the detection, mapping and analysis of phytoplankton blooms in coastal and open oceans. *Progress in Oceanography* **123(2)**:123–144 DOI 10.1016/j.pocean.2013.12.008.

Botella JA, Ulschmid JK, Gruenewald C, Moehle C, Kretzschmar D, Becker K, Schneuwly S. 2004. The *Drosophila* carbonyl reductase sniffer prevents oxidative stress-induced neurodegeneration. *Current Biology* **14(9)**:782–786 DOI 10.1016/j.cub.2004.04.036.

Carnevale C, Finzi G, Pisoni E, Volta M. 2009. Neuro-fuzzy and neural network systems for air quality control. *Atmospheric Environment* **43(31)**:4811–4821 DOI 10.1016/j.atmosenv.2008.07.064.

Casolaro A, Capone V, Camastra F. 2025. Predicting ground-level nitrogen dioxide concentrations using the Bayesian attention-based deep neural network. *Ecological Informatics* **87(4)**:103097 DOI 10.1016/j.ecoinf.2025.103097.

Casolaro A, Capone V, Iannuzzo G, Camastra F. 2023. Deep learning for time series forecasting: advances and open problems. *Information* **14(11)**:598 DOI 10.3390/info14110598.

Chu HT, Ge L, Ng A, Rizos C. 2012. Application of genetic algorithm and support vector machine in classification of multisource remote sensing data. *International Journal of Remote Sensing Applications* **2(3)**:1–11.

Donmez C, Villi O, Berberoglu S, Cilek A. 2021. Computer vision-based citrus tree detection in a cultivated environment using UAV imagery. *Computers and Electronics in Agriculture* **187**:106273 DOI 10.1016/j.compag.2021.106273.

Duan W, Maskey S, Chaffe PLB, Luo P, He B, Wu Y, Hou J. 2021. Recent advancement in remote sensing technology for hydrology analysis and water resources management. *Remote Sensing* **13(6)**:1097 DOI 10.3390/rs13061097.

Ekstrom PA, Hales JM. 2000. A wavelet–based approach for atmospheric pollution modeling: algorithm development. *Monthly Weather Review* **128(9)**:3169–3186 DOI 10.1175/1520-0493(2000)128<3169:oddwfs>2.0.co;2.

Ghahremanloo M, Lops Y, Choi Y, Yeganeh B. 2021. Deep learning estimation of daily ground-level NO_2 concentrations from remote sensing data. *Journal of Geophysical Research: Atmospheres* **126(21)**:e2021JD034925 DOI 10.1029/2021jd034925.

He Z, Guo Q, Wang Z, Li X. 2025. A hybrid wavelet-based deep learning model for accurate prediction of daily surface PM2.5 concentrations in Guangzhou city. *Toxics* **13(4)**:254 DOI 10.3390/toxics13040254.

Huang Y, Lin G, Chen D, Zhao W. 2024. Deep neural-fuzzy system algorithms with improved interpretability for classification problems. *International Journal of Fuzzy Systems* **26(3)**:900–921 DOI 10.1007/s40815-023-01642-7.

Ito K, Biljecki F. 2021. Assessing bikeability with street view imagery and computer vision. *Transportation Research Part C: Emerging Technologies* **132**:103371 DOI 10.1016/j.trc.2021.103371.

Jeong S, Ko J, Shin T, Yeom J-M. 2022. Incorporation of machine learning and deep neural network approaches into a remote sensing-integrated crop model for the simulation of rice growth. *Scientific Reports* **12(1)**:9030 DOI 10.1038/s41598-022-13232-y.

Kattenborn T, Leitloff J, Schiefer F, Hinz S. 2021. Review on convolutional neural networks (CNN) in vegetation remote sensing. *ISPRS Journal of Photogrammetry and Remote Sensing* **173(2)**:24–49 DOI 10.1016/j.isprsjprs.2020.12.010.

Khatri N, Tyagi S. 2015. Influences of natural and anthropogenic factors on surface and groundwater quality in rural and urban areas. *Frontiers in Life Science* **8(1)**:23–39 DOI 10.1080/21553769.2014.933716.

Leitgib L, Kálmán J, Gruiz K. 2007. Comparison of bioassays by testing whole soil and their water extract from contaminated sites. *Chemosphere* **66(3)**:428–434 DOI 10.1016/j.chemosphere.2006.06.024.

Liang S. 2005. *Quantitative remote sensing of land surfaces*. Hoboken: John Wiley & Sons.

Lin Z, Zhang G. 2020. Genetic algorithm-based parameter optimization for EO-1 Hyperion remote sensing image classification. *European Journal of Remote Sensing* **53(1)**:124–131 DOI 10.1080/22797254.2020.1747949.

Malik DS, Shah T, Tehsin S, Nasir IM, Fitriyani NL, Syafrudin M. 2024. Block cipher nonlinear component generation via hybrid pseudo-random binary sequence for image encryption. *Mathematics* **12(15)**:2302 DOI 10.3390/math12152302.

Marini F, Walczak B. 2015. Particle swarm optimization (PSO). A tutorial. *Chemometrics and Intelligent Laboratory Systems* **149**:153–165 DOI 10.1016/j.chemolab.2015.08.020.

Mudassar S, Zameer A, Rehman A, Nasir R, Raja MAZ. 2026. A two-stage convolutional gated recurrent unit with multi-head attention and regularization for multi-step ahead prediction of particulate air pollutants. *The European Physical Journal Plus* **141(1)**:22 DOI 10.1140/epjp/s13360-025-07234-8.

Najafabadi MM, Villanustre F, Khoshgoftaar TM, Seliya N, Wald R, Muharemagic E. 2015. Deep learning applications and challenges in big data analytics. *Journal of Big Data* **2(1)**:1–21 DOI 10.1186/s40537-014-0007-7.

Nasir IM, Tehsin S, Damaševičius R, Maskeliūnas R. 2024a. Integrating explanations into CNNs by adopting spiking attention block for skin cancer detection. *Algorithms* **17(12)**:557 DOI 10.3390/a17120557.

Nasir IM, Tehsin S, Damaševičius R, Zielonka A, Woźniak M. 2024b. Explainable cubic attention-based autoencoder for skin cancer classification. In: *International Conference on Artificial Intelligence and Soft Computing*. Cham: Springer, 124–134.

Pang Y, Yao L, Luo Y, Dong C, Kong Q, Chen B. 2024. RepSViT: an efficient vision transformer based on spiking neural networks for object recognition in satellite on-orbit remote sensing images. *IEEE Transactions on Geoscience and Remote Sensing* **62(6)**:1–16 DOI 10.1109/tgrs.2024.3367709.

Park K, Lee EH. 2024. Urban flood vulnerability analysis and prediction based on the land use using deep neural network. *International Journal of Disaster Risk Reduction* **101(1–4)**:104231 DOI 10.1016/j.ijdrr.2023.104231.

Rajeena F, Tehsin S. 2025. A framework for breast cancer classification with deep features and modified grey wolf optimization. *Mathematics* **13(8)**:1236 DOI 10.3390/math13081236.

San-Miguel-Ayanz J, Ravail N. 2005. Active fire detection for fire emergency management: potential and limitations for the operational use of remote sensing. *Natural Hazards* **35(3)**:361–376 DOI 10.1007/s11069-004-1797-2.

Shirin S, Ansari MI, Pandey G, Sharma SN, Yadav AK. 2023. Fuzzy and neural network model-based environmental quality monitoring system. In: *Modeling and Simulation of Environmental Systems*. Boca Raton: CRC Press.

Siam ZS, Hasan RT, Anik SS, Noor F, Adnan MSG, Rahman RM, Dewan A. 2022. National-scale flood risk assessment using GIS and remote sensing-based hybridized deep neural network and fuzzy analytic hierarchy process models: a case of Bangladesh. *Geocarto International* **37(26)**:12119–12148 DOI 10.1080/10106049.2022.2063411.

Tehsin S, Hassan A, Riaz F, Nasir IM, Fitriyani NL, Syafrudin M. 2024. Enhancing signature verification using triplet siamese similarity networks in digital documents. *Mathematics* **12(17)**:2757 DOI 10.3390/math12172757.

Tehsin S, Nasir IM, Damaševičius R. 2024. Explainability of disease classification from medical images using XGrad-Cam. In: *International Conference on Advanced Research in Technologies, Information, Innovation and Sustainability*. Cham: Springer, 221–236.

Tian H, Wang T, Liu Y, Qiao X, Li Y. 2020. Computer vision technology in agricultural automation—a review. *Information Processing in Agriculture* **7(1)**:1–19 DOI 10.1016/j.inpa.2019.09.006.

Wang Y. 2024. Optimizing convolutional neural networks using elitist firefly algorithm for remote sensing classification. *Evolutionary Intelligence* **17(4)**:1–14 DOI 10.1007/s12065-024-00913-y.

Wang G, Qiao J. 2021. An efficient self-organizing deep fuzzy neural network for nonlinear system modeling. *IEEE Transactions on Fuzzy Systems* **30(7)**:2170–2182 DOI 10.1109/tfuzz.2021.3077396.

Yousafzai SN, Nasir IM, Tehsin S, Fitriyani NL, Syafrudin M. 2025a. FLTrans-Net: transformer-based feature learning network for wheat head detection. *Computers and Electronics in Agriculture* **229(12)**:109706 DOI 10.1016/j.compag.2024.109706.

Yousafzai SN, Nasir IM, Tehsin S, Malik DS, Keshta I, Fitriyani NL, Gu Y, Syafrudin M. 2025b. Multi-stage neural network-based ensemble learning approach for wheat leaf disease classification. *IEEE Access* **13**:30101 DOI 10.1109/ACCESS.2025.3541347.